

Synthetic Humans for Action Recognition from Unseen Viewpoints

Gül Varol^{1,*}Ivan Laptev^{2,3}Cordelia Schmid^{2,4}Andrew Zisserman¹¹University of Oxford²Inria³École Normale Supérieure⁴Google AI

Abstract

Our goal in this work is to improve the performance of human action recognition for viewpoints unseen during training by using synthetic training data. Although synthetic data has been shown to be beneficial for tasks such as human pose estimation, its use for RGB human action recognition is relatively unexplored. We make use of the recent advances in monocular 3D human body reconstruction from real action sequences to automatically render synthetic training videos for the action labels.

We make the following contributions: (i) we investigate the extent of variations and augmentations that are beneficial to improving performance at new viewpoints. We consider changes in body shape and clothing for individuals, as well as more action relevant augmentations such as non-uniform frame sampling, and interpolating between the motion of individuals performing the same action; (ii) We introduce a new dataset, SURREACT, that allows supervised training of spatio-temporal CNNs for action classification; (iii) We substantially improve the state-of-the-art action recognition performance on the NTU RGB+D and UESTC standard human action multi-view benchmarks; Finally, (iv) we extend the augmentation approach to in-the-wild videos from a subset of the Kinetics dataset to investigate the case when only one-shot training data is available, and demonstrate improvements in this case as well.

1. Introduction

Learning human action representations from RGB video data has been widely studied. Recent advances on convolutional neural networks (CNNs) [32] have shown excellent performance [6, 14, 15, 17, 35, 76] on benchmark datasets, such as UCF101 [66]. However, the success of CNNs rely heavily on the availability of large-scale training data, which is not always the case. To address the lack of training data, several works explore the use of complementary synthetic data for a range of tasks in computer vision such as optical flow estimation, segmentation, human body and hand pose estimation [11, 64, 67, 73, 85]. In this work,

*Work partially done at Inria and during an internship at Google AI.

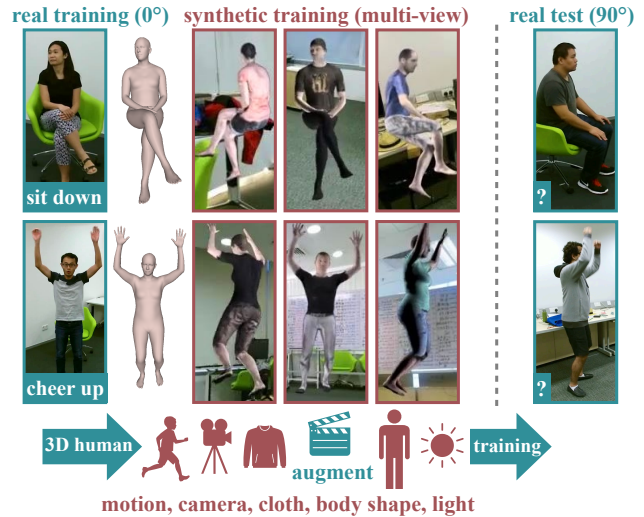


Figure 1. We estimate 3D shape from real videos and automatically render synthetic videos with action labels. We explore various augmentations for motions, viewpoints, and appearance. Training temporal CNNs with this data significantly improves the action recognition from unseen viewpoints.

we raise the question *how to synthesize videos for action recognition* in the case of limited real data, such as only one viewpoint, or one-shot available at training.

Imagine a surveillance or ambient assisted living system, where a dataset is already collected for a set of actions from a certain camera. Placing a new camera in the environment from a new viewpoint would require re-annotating data because the appearance of an action is drastically different when performed from different viewpoints [23, 38, 84]. In fact, we observe that state-of-the-art action recognition networks fail drastically when trained and tested on distinct viewpoints. Specifically, we train the network architecture of [17] on videos from a benchmark dataset NTU RGB+D [63] where people are facing the camera. When we test this network on other front-view (0°) videos, we obtain $\sim 80\%$ accuracy. When we test with side-view (90°) videos, the performance drops to $\sim 40\%$ (see Section 4). This motivates us to study action recognition from novel viewpoints.

Existing methods addressing cross-view action recognition do not work in challenging setups (e.g. same subjects

and similar viewpoints in training and test splits [63]). We introduce and study a more challenging protocol with only one viewpoint at training. Recent methods assuming multi-view training data [33, 34, 74] also become inapplicable.

A naive way to achieve generalization is to collect data from all views, for all possible conditions, but this is impractical due to combinatorial explosion [80]. Instead, we augment the existing real data synthetically to increase the diversity in terms of viewpoints, appearance, and motions. Synthetic humans are relatively easy to render for tasks such as pose estimation, because arbitrary motion capture (MoCap) resource can be used [64, 73]. However, action classification requires certain motion patterns and semantics. It is challenging to generate synthetic data with action labels [9]. Typical MoCap datasets [1], targeted for pose diversity, are not suitable for action recognition due to lack of clean action annotations. Even if one collects a MoCap dataset, it is still limited to the pre-defined set of categories.

In this work, we propose an efficient and scalable approach for generating *synthetic videos with action labels* from the target set of categories. We employ a 3D human shape estimation method, HMMR [25], that automatically extracts the 3D human dynamics from a single-view RGB video. The resulting sequence of SMPL body [44] pose parameters are then combined with other randomized generation components (e.g. viewpoint, clothing) to render diverse complementary training data with action annotations. Figure 1 presents an overview of our pipeline. We demonstrate the advantages of such data when training spatio-temporal CNN models for (i) action recognition from unseen viewpoints and (ii) training with one-shot real data. We boost performance on unseen viewpoints from 53.6% to 67.1% on NTU, and from 49.4% to 67.8% on UESTC dataset by augmenting limited real training data with our proposed SURREACT dataset. Furthermore, we present an in-depth analysis about the importance of action relevant augmentations such as diversity of motions and viewpoints, as well as our non-consecutive frame sampling strategy which substantially improves the action recognition performance. Our code and data will be publicly available at [68].

2. Related Work

Action recognition is a well-established research field. For a broad review of the literature, see the recent survey of Kong et al. [30]. Here, we focus on relevant works on synthetic data and cross-view action recognition.

Synthetic humans. Simulating human actions date back to 1980s. Badler et al. [2] provide an extensive overview of early approaches. More recently, synthetic images of people have been used to train visual models for 2D/3D body pose and shape estimation [7, 16, 36, 53, 64, 72], part segmentation [64, 73], depth estimation [73], multi-person pose estimation [20], pedestrian detection [48, 53], person re-

identification [56], hand pose estimation [18, 85], and face recognition [49]. Synthetic datasets built for these tasks, such as the recent SURREAL dataset [73], however, do not provide action labels.

Among previous works that focus on synthetic human data, very few tackle action recognition [9, 37, 59]. Synthetic 2D human pose sequences [47] and synthetic point trajectories [58, 60] have been used for view-invariant action recognition. However, RGB-based synthetic training for action recognition is relatively new, with [9] being one of the first attempts. De Souza et al. [9] manually define 35 action classes and jointly estimate real categories and synthetic categories in a multi-task setting. However, their categories are not easily scalable and do not necessarily relate to the target set of classes. Unlike [9], we automatically extract motion sequences from real data, making the method flexible for new categories. Recently, [55] has generated the VirtualHome dataset, a simulation environment with programmatically defined synthetic activities using crowdsourcing. Different than our work, the focus of [55] is not generalization to real data.

Most relevant to ours, [37] generates synthetic training images to achieve better performance on unseen viewpoints. The work of Liu et al. [37] is an extension of [59] by using RGB-D as input instead of depth only. Both works formulate a frame-based pose classification problem on their synthetic data, which they then use as features for action recognition. These features are not necessarily discriminative for the target action categories. Different than this direction, we explicitly assign an action label to synthetic videos and define the supervision directly on action classification.

Cross-view action recognition. Due to the difficulty of building multi-view action recognition datasets, the standard benchmarks have been recorded in controlled environments. RGB-D datasets such as IXMAS [77], UWA3D II [57] and N-UCLA [75] were state of the art until the availability of the large-scale NTU RGB+D dataset [63]. The size of NTU allows training deep neural networks unlike previous datasets. Very recently, Ji et al. [22] collected the first large-scale dataset, UESTC, that has a 360° coverage around the performer, although still in a lab setting.

Since multi-view action datasets are typically captured with depth sensing devices, such as Kinect, they also provide an accurate estimate of the 3D skeleton. Skeleton-based cross-view action recognition therefore received a lot of attention in the past decade [27, 39, 40, 41, 82]. Variants of LSTMs [19] have been widely used [39, 40, 63]. Recently, spatio-temporal skeletons were represented as images [27] or higher dimensional objects [41] where standard CNN architectures were applied.

RGB-based cross-view action recognition is in comparison less studied. Transforming RGB features to be view-invariant is not as trivial as transforming 3D skeletons.

Early work on transferring appearance features from the source view to the target view explored the use of maximum margin clustering to build a joint codebook for temporally synchronous videos [13]. Following this approach, several other works focused on building global codebooks to extract view-invariant representations [29, 43, 60, 83, 84]. Recently, end-to-end approaches used human pose information as guidance for action recognition [3, 42, 46, 86]. Li et al. [33] formulated an adversarial view-classifier to achieve view-invariance. Wang et al. [74] proposed to fuse view-specific features from a multi-branch CNN. Such approaches cannot handle single-view training [33, 74]. Our method differs from these works by compensating for the lack of view diversity with synthetic videos. Our method is conceptually simple, but effective. We augment the real data automatically at training time, and our model does not involve any extra cost at test time unlike [74]. Moreover, we do not assume real multi-view videos at training.

3D human shape estimation. Recovering the full human body mesh from a single image has been explored as a model-fitting problem [5, 31], as regressing model parameters with CNNs [24, 51, 52, 71], and as regressing non-parametric representations such as graphs or volumes [28, 72]. Recently, CNN-based parameter regression approaches have been extended to video [25, 36]. HMMR [25] learns the human dynamics by using 1D temporal convolutions. In this work, we adopt this method for recovering 3D body parameters from real videos.

3. Synthetic humans with action labels

Our goal is to improve the performance of action recognition for viewpoints unseen during training using synthetic data. In the following, we describe the three stages of: (i) obtaining 3D temporal models for human actions from real training sequences (at a particular viewpoint) (Section 3.1); (ii) using these 3D temporal models to generate training sequences for new (and the original) viewpoints using a rendering pipeline with augmentation (Section 3.2); and (iii) training a spatio-temporal CNN with this real and synthetic data (Section 3.3).

3.1. 3D human motion estimation

In order to generate a synthetic video with graphics techniques, we need to have a sequence of articulated 3D human body models. We employ the parametric body model SMPL [44], which is a statistical model, learned over thousands of 3D scans. SMPL generates the mesh of a person given the disentangled pose and shape parameters. The pose parameters (\mathbb{R}^{72}) control the kinematic deformations due to skeletal posture, while the shape parameters (\mathbb{R}^{10}) control identity-specific deformations such as the person height.

We hypothesize that a human action can be captured by the sequence of *pose* parameters. We assume that if we

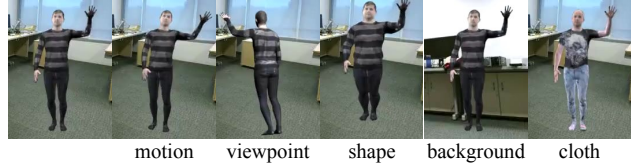


Figure 2. We illustrate different augmentations of the SURREACT dataset for the hand waving action. We modify the joint angles with additive noise on the pose parameters for *motion* augmentation. We systematically change the camera position to create *viewpoint* diversity. We sample from a large set of body *shape* parameters, *backgrounds*, and *clothing* to randomize appearances.

can predict reliable 3D pose sequences from action recognition video datasets, we can transfer the associated action labels to synthetic videos. We use the recent method of Kanazawa et al. [25], namely human mesh and motion recovery (HMMR). HMMR extends the single-image reconstruction method HMR [24] to video with a multi-frame CNN that takes into account a temporal neighborhood around a video frame. HMMR learns a temporal representation for human dynamics by incorporating large-scale 2D pseudo-ground truth poses for in-the-wild videos. It uses PoseFlow [81] and AlphaPose [12] for multi-person 2D pose estimation and tracking as a pre-processing step. Each person crop is then given as input to the CNN for estimating the pose and shape, as well as the weak-perspective camera parameters. We refer the reader to [25] for more details. We choose this method for the robustness on in-the-wild videos, ability to capture multiple people, and the smoothness of the recovered motion, which are important for our generalization from synthetic videos to real. Figure 1 presents the 3D pose animated synthetically for sample video frames. Note that we only use the pose parameters from HMMR, and randomly change the shape parameters, camera parameters, and other factors. Next, we present the augmentations in our synthetic data generation.

3.2. SURREACT dataset components

In this section, we give details on our synthetic dataset, SURREACT (Synthetic hUmans foR Real ACTions). We follow [73] and render 3D SMPL sequences with randomized cloth textures, lighting, and body shapes. We animate the body model with our automatically extracted pose dynamics as described in the previous section. We explore various *motion augmentation* techniques to increase intra-class diversity in our training videos. We incorporate *multi-person* videos which are especially important for two-people interaction categories. We also systematically sample from 8 *viewpoints* around a circle to perform controlled experiments. Different augmentations are illustrated in Figure 2 for a sample synthetic frame. Each generated video has automatic ground truth for 3D joint locations, part segmentation, optical flow, and SMPL body [44] parameters, as well as an action label, which we use for training a video-

based 3D CNN for action classification. Our new SUR-REACT dataset differs from the SURREAL dataset [73] mainly by providing action labels and by using automatically extracted motion sequences instead of MoCap recordings [1]. Consequently, Varol et al. [73] do not exploit the temporal aspect of their dataset, but only train CNNs with single-image input. We further employ multi-person videos and a systematic viewpoint distribution.

Motion augmentation. Automatic extraction of 3D sequences from 2D videos poses an additional challenge in our dataset compared to clean high-quality MoCap sequences. To reduce the jitter, we temporally smooth the estimated SMPL pose parameters by weighted linear averaging. SMPL poses are represented as axis-angle rotations between joints. We convert them into quaternions when we apply linear operations, then normalize each quaternion to have a unit norm, before converting back to axis-angles.

To increase motion diversity, we further perturb the pose parameters with various augmentations. Specifically, we use a video-level *additive noise* on the quaternions for each body joint to slightly change the poses, as an intra-individual augmentation. We also experiment with an inter-individual augmentation by interpolating between motion sequences of the same action class. Given a pair of sequences from two individuals, we first align them with dynamic time warping [62], then we linearly interpolate the quaternions of the time-aligned sequences to generate a new sequence, which we refer as *interpolation*. We show significant gains by increasing motion diversity.

Multi-person. We use the 2D pose information from [12, 81] to count the number of people in the real video. In the case of a single-person, we center the person on the image and do not add 3D translation to the body. If there is more than one person, we insert additional body model(s) for rendering. We translate each person in the xy image plane. Note that we do not translate the person in full xyz space. We observe that the z component of the translation estimation is not reliable due to the depth ambiguity therefore the people are always centered at $z = 0$. More explanations about the reason for omitting the z component can be found in Appendix A. We temporally smooth the translations to reduce the noise. We subtract the mean of translations across the video and across the people to roughly center all people to the frame. We therefore keep the relative distances between people, which is important for actions such as *walking towards each other*.

Viewpoints. We systematically render each motion sequence 8 times by randomizing all other generation parameters at each view. In particular, we place the camera to be rotated at $\{0^\circ, 45^\circ, 90^\circ, 135^\circ, 180^\circ, 225^\circ, 270^\circ, 315^\circ\}$ azimuth angles with respect to the origin, denoted as $(0^\circ:45^\circ:360^\circ)$ in our experiments. The distance of the camera from the origin and the height of the camera from the

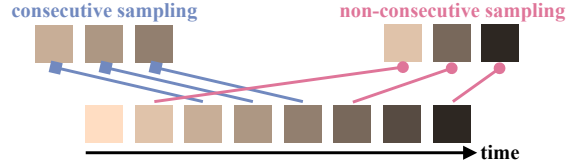


Figure 3. We illustrate our non-consecutive frame sampling strategy in our 3D CNN training. Compared to the commonly adopted consecutive setting which uniformly samples with a fixed frame rate, non-consecutive sampling has random skips in time, allowing speed augmentations and long-term context.

ground are randomly sampled from a predefined range: $[4, 6]$ meters for the distance, $[-1, 3]$ meters for the height.

Backgrounds. Since we have access to the target real dataset where we run pose estimation methods, we can extract background pixels directly from the training set of this dataset. We crop from regions without the person to obtain static backgrounds for the NTU and UESTC datasets. For Kinetics experiments, we use unconstrained videos from non-overlapping action classes. We render human bodies on top of these 2D backgrounds.

3.3. Training 3D CNNs with non-consecutive frames

Following the success of 3D CNNs for video recognition [6, 17, 70], we employ a spatio-temporal convolutional architecture that operates on multi-frame video inputs. Unless otherwise specified, our network architecture is 3D ResNet-50 [17] and its weights are randomly initialized.

To study the generalization capability of synthetic data across different input modalities, we train one CNN for RGB and another for optical flow as in [65]. We average the scores when reporting the fusion.

We subsample fixed-sized inputs from videos to have a $16 \times 256 \times 256$ spatio-temporal resolution, in terms of number of frames, width, and height, respectively. In case of optical flow input, we map the RGB input to $15 \times 64 \times 64$ dimensional flow estimates. For this, we train a two-stack hourglass architecture [50] with our synthetic data for flow estimation on 2 consecutive frames.

Frame sampling. We adopt a different frame sampling strategy than most works [6, 14, 17]. Instead of uniformly sampling (at a fixed frame rate) a video clip with consecutive frames, we randomly sample frames across time by keeping their temporal order, which we refer as *non-consecutive* sampling. Although recent works explore multiple temporal resolutions, e.g. by regularly sampling at two different frame rates [14], the sampled frames are equidistant from each other. TSN [76] employs a hybrid strategy by regularly sampling temporal segments and randomly sampling a frame from each segment, but TSN uses a 2D CNN without temporal modelling. Figure 3 compares the consecutive sampling with our proposed non-consecutive sampling. In our experiments, we report results for both and show improvements for the latter. Our videos are tempo-



Figure 4. We show samples from the multi-view datasets used in our experiments. NTU and UESTC datasets have 3 and 8 viewpoints, respectively. NTU views correspond to 0° , 45° , and 90° from left to right. UESTC covers 360° around the performer.

rally trimmed around the action, therefore, each video is short, i.e. spans several seconds. During training we randomly sample 16 frames from a video as a fixed-sized input to 3D CNN. Thus, our convolutional kernels become speed-invariant to some degree. This can be seen as a data augmentation technique, as well as a way to capture long-term cues. At test time, we sample several 16-frame clips and average the softmax scores. If we test the consecutive case, we sample non-overlapping consecutive clips with sliding window. For the non-consecutive case, we randomly sample as many non-consecutive clips as the number of sliding windows for the former case. In other words, the number of sampled clips is proportional to the video length. We observe that it is important to train and test with the same sampling, and keeping the temporal order is important. More details can be found in Appendix B.3.

Synth+Real. Since each real video is augmented multiple times (e.g. 8 times for 8 views), we have more synthetic data than real. When we add synthetic data to training, we balance the real and synthetic datasets such that at each epoch we randomly subsample from the synthetic videos to have equal number for both real and synthetic.

We minimize the cross-entropy loss using RMSprop [69] with mini-batches of size 10 and an initial learning rate of 10^{-3} with a fixed schedule. Color augmentation is used for the RGB stream. Other implementation details are given in Appendix A.

4. Experiments

In this section, we start by presenting the datasets used in our experiments (Section 4.1). Then, we present our results on unseen viewpoints (Section 4.2). Finally, we illustrate our approach on in-the-wild videos (Section 4.3).

4.1. Datasets and evaluation protocols

NTU RGB+D dataset (NTU). This dataset [63] captures 60 actions with 3 synchronous cameras (see Figure 4). The large scale (56K videos) of the dataset allows training deep neural networks. Each sequence has 84 frames on average. The standard protocols [63] report accuracy for cross-view and cross-subject splits. The cross-view (CV) split considers 0° and 90° views as training and 45° view as test, and the same subjects appear both in training and test. For the cross-subject (CS) setting, 20 subjects are used for training, the remaining 20 for test, and all 3 views are seen at both training and test. We report on the standard protocols to be

able to compare to the state of the art (see Table 7). However, we introduce a new protocol to make the task more challenging. From the cross-subject training split that has all 3 views, we take only 0° viewpoint for training, and we test on the 0° , 45° , 90° views of the cross-subject test split. We call this protocol cross-view-subject (CVS). Our focus is mainly to improve for the unseen and distinct view of 90° .

UESTC RGB-D varying-view 3D action dataset (UESTC). UESTC is a recent dataset [22] that systematically collects 8 equally separated viewpoints that cover 360° around a person (see Figure 4). In total, the dataset has 118 subjects, 40 actions categories, and 26500 videos of more than 200 frames each. This dataset allows studying actions from unusual views such as behind the person. We use the official protocol Cross View I (CV-I), suitable for our task, which trains with 1 viewpoint and tests with all other 7 for each view. The final performance is evaluated as the average across all tests. The official Cross View II (CV-II) protocol concentrates on multi-view training, which reports training with even viewpoints (FV, V2, V4, V6) and testing with odd viewpoints (V1, V3, V5, V7), and vice versa. We report on the first split.

One-shot Kinetics-15 dataset (Kinetics-15). Since we wish to formulate a one-shot scenario from in-the-wild Kinetics [26] videos, we need a pre-trained model to serve as feature extractor. We use a model pre-trained on Mini-Kinetics-200 [78], a subset of Kinetics-400. We define the novel classes from the remaining 200 categories which can be described by body motions. This procedure resulted in a 15-class subset of Kinetics-400: *bending back*, *clapping*, *climbing a rope*, *exercising arm*, *hugging*, *jogging*, *jumpstyle dancing*, *krumping*, *push up*, *shaking hands*, *skip-ping rope*, *stretching arm*, *swinging legs*, *sweeping floor*, *wrestling*. Note that many of the categories such as *waiting in line*, *dining*, *holding snake* cannot be recognized solely by their body motions, but additional contextual cues are needed. From the 15 actions, we randomly sample 1 training video per class (see Figure 6 for example videos with their synthetic augmentations). For testing, we report accuracy on all 725 validation videos.

4.2. Action recognition from unseen viewpoints

We first compare real-only (Real), synthetic-only (Synth), and mixed synthetic and real (Synth+Real) training. Next, we experiment with the different synthetic data generation parameters to analyze the effects of viewpoint

Training Views	Test Views					
	consecutive			non-consecutive		
	0°	45°	90°	0°	45°	90°
0°	83.9	67.9	42.9	86.9	74.5	53.6
45°	72.1	81.6	66.8	78.1	85.2	75.7
90°	41.7	63.4	81.4	52.3	71.2	85.4
0° + 45°	86.0	85.3	69.9	89.7	88.9	79.3
0° + 45° + 90°	86.8	86.9	84.1	89.4	89.4	87.8

Table 1. Training and testing with our cross-view-subject (CVS) protocol of the NTU dataset using only real RGB videos. Training and testing on the same viewpoint shows the best performance as can be seen by the diagonals of the first three rows. This shows the domain gap present between 0°, 45°, 90° viewpoints. If we add more viewpoints to the training (last two rows) we account for the domain gap. Non-consecutive frame sampling (right) consistently outperforms the consecutive frame sampling (left).

Training data	seen view	unseen views	
	0°	45°	90°
Synth(0°:45°:360°)	54.0	49.5	42.7
Real(0°)	86.9	74.5	53.6
Real(0°) + Synth(0°:45°:360°)	89.1	82.0	67.1

Table 2. Training jointly on synthetic and real data substantially boosts the performance compared to only real training on NTU CVS protocol, especially on unseen views (e.g. 67.1% vs 53.6%). Training on synthetic videos alone obtains about 50% accuracy.

and motion diversity. Then, we compare our results with the state of the art. In all cases, we evaluate our models on real test videos.

Real baselines. We start with our cross-view-subject protocol on NTU by training only with real data. Table 1 summarizes the results of training the model on a single-view and testing on all views. First, we note the consistent improvement of non-consecutive frame sampling in all settings. Second, we observe a clear domain gap between different viewpoints, which can be addressed by adding more views in training. However, in the case when a single view is available, this would not be possible. In the remaining of our experiments on NTU, we assume that only the frontal viewpoint (0°) is available. Next, we report the improvements obtained by synthetically increasing view diversity.

Synth+Real training. We train the 60 action classes from NTU by combining the real 0° training data and the synthetic data augmented from real with 8 viewpoints, i.e. 0°:45°:360°. Table 2 presents the results of the RGB stream. It is interesting to note that training only with synthetic data reaches 54% accuracy on real 0° test data which indicates a certain level of generalization capability from synthetic to real. Combining real and synthetic training videos, the performance increases from 53.6% to 67.1% compared to only real training, on the challenging unseen 90° viewpoint. Note that the additional synthetic videos can be obtained ‘for free’, i.e. without extra annotation cost.

The advantage of having a controllable data generation procedure is to be able to analyze what components of the

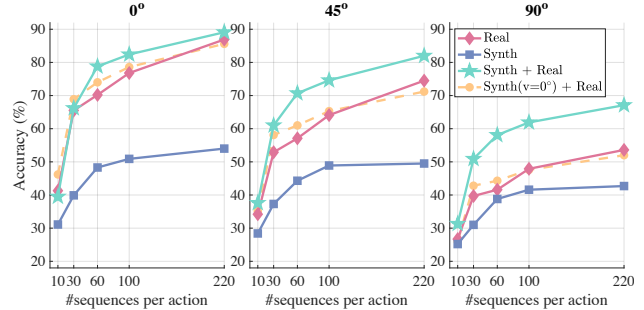


Figure 5. The number of real sequences per action for: Real, Synth, Synth+Real training on NTU CVS split. Generalization to unseen viewpoints is significantly improved with the addition of synthetic data (green) compared to training only with real (pink). Real training contains the 0° view. We experiment with all 8 views (green) or only the 0° view (yellow) in the additional synthetic data. See text for interpretation.

	0°	45°	90°
Synth(0°)	38.3	27.1	17.9
Synth(45°, 315°)	35.9	34.2	26.8
Synth(90°, 270°)	13.9	18.3	23.2
Synth(0°:45°:360°)	48.3	44.3	38.8

Table 3. The effect of the viewpoints in the synthetic training on the NTU CVS split. We train only with synthetic videos obtained from real data of 60 sequences per action. We take a subset of views from the synthetic data: 0°, ±45°, ±90°. Even when synthetic, the performance is better when the viewpoints match between training and test (highlighted diagonal). The best performance is obtained with all 8 viewpoints combined.

synthetic data are important. In the following, we examine a few of these aspects, such as amount of data, view diversity, and motion diversity. Additional results and illustrations can be found in Appendices B and C.

Amount of data. In the NTU CVS training split, we have about 220 sequences per action. We take subsets with {10, 30, 60, 100} sequences per action, and train the three scenarios: Real, Synth, Synth+Real, for each subset. Figure 5 plots the performance versus the amount of data for these scenarios. We observe the consistent improvement of complementary synthetic training, especially for unseen viewpoints. We also see that it is more effective to use synthetic data at a given number of sequences per action. For example, on the 90° viewpoint, increasing the number of sequences from 100 to 220 in the real data results only in 4.6% improvement (49.0% vs 53.6%, Real), while one can synthetically augment the existing 100 sequences per action and obtain 64.7% (Synth+Real) accuracy without spending extra annotation effort for real data. We draw the same conclusion with optical flow input in Appendix B.1.

View diversity. We wish to confirm that the improvements presented so far are mainly due to the viewpoint variation in synthetic data. The ‘‘Synth(v=0°) + Real’’ plot in Figure 5 indicates that only the 0° viewpoint from synthetic data is used. In this case, we observe that the improvement is

#sequences per action	#renders	motion augmentation	Test views		
			0°	45°	90°
10	1	-	31.1	28.4	25.2
10	6	-	33.1	31.6	26.2
10	6	interpolation	35.7	31.5	26.9
10	6	additive noise	37.9	35.9	31.5
60	1	-	48.3	44.3	38.8

Table 4. The effect of motion diversity in the synthetic training on the NTU CVS split. The results indicate that clothing, body shape diversity is not as important as motion diversity (second and last rows). We can significantly improve the performance by motion augmentations, especially with additive noise on the joint rotations (second and fourth rows). Here, each dataset is rendered with all 8 views and the training is only performed on synthetic data. At each rendering, we randomly sample clothing, body shape, lighting etc.

not consistent. Therefore, it is important to augment viewpoints to obtain improvements. Moreover, we experiment with having only $\pm 45^\circ$ or $\pm 90^\circ$ views in the synthetic-only training for 60 sequences per action. In Table 3, we observe that the test performance is higher when the synthetic training view matches the real test view. However, having all 8 viewpoints at training benefits all test views.

Motion diversity. Next, we investigate the question whether motions can be diversified and whether this is beneficial for synthetic training. There are very few attempts towards this direction [9] since synthetic data has been mainly used for static images. Recently, [36] introduced interpolation between distinct poses to create new poses in synthetic data for training 3D pose estimation; however, its contribution over existing poses was not experimentally validated. In our case, we need to preserve the action information, therefore, we cannot generate unconstrained motions. Generating realistic motions is a challenging research problem on its own and is out of the scope of this paper. Here, we experiment with motion augmentation to increase diversity.

As explained in Section 3.1, we generate new motion sequences by (i) interpolating between motion pairs of the same class, or by (ii) additive noise on the pose parameters. Table 4 presents the results of this analysis when we train only with synthetic data and test on the NTU CVS protocol. We compare to the baseline where 10 motion sequences per action are rendered once per viewpoint (the first row). We render the same sequences without motion augmentation 6 times (the second row) and obtain marginal improvement. On the other hand, having 60 real motion sequences per action significantly improves (last row) and is our upper bound for the motion augmentation experiments. That means that the clothing, body shape, lighting, i.e. appearance diversity is not as important as motion diversity. We see that generating new sequences with interpolations improves over the baseline. Moreover, perturbing the joint rotations across the video with additive noise is simple and effective, with performance increase of about 5% (26.2% vs 31.5%) over rendering 6 times without motion augmentation.

Real (Avg 49.4%)								Synth+Real (Avg 67.8%)									
	FV	V1	V2	V3	V4	V5	V6	V7		FV	V1	V2	V3	V4	V5	V6	V7
FV	76.1	25.9	57.4	74.4	65.6	27.6	61.6		FV	86.8	42.4	72.9	81.1	77.4	44.1	82.5	
V1	53.5	48.9	68.1	56.9	64.2	37.8	80.4		V1	72.8	58.2	79.3	69.7	82.3	56.5	83.6	
V2	14.0	39.9	42.1	27.6	26.1	70.9	34.3		V2	47.8	72.8	65.2	44.6	63.2	84.2	70.0	
V3	35.9	73.5	38.1	63.2	72.4	27.8	68.4		V3	61.5	83.8	61.2	73.5	84.5	57.4	80.9	
V4	48.1	54.1	24.4	65.7	66.4	23.2	46.7		V4	68.6	73.9	44.9	72.1	77.9	40.9	67.9	
V5	19.6	59.1	23.3	70.4	67.0	29.8	64.1		V5	67.4	83.7	50.9	85.3	78.6	53.6	76.2	
V6	16.6	27.9	74.9	44.0	23.9	42.6	31.5		V6	45.4	69.3	86.8	66.4	48.5	66.9	70.1	
V7	53.3	83.9	35.9	75.9	52.4	72.4	36.6		V7	65.0	83.3	53.2	76.8	61.3	71.8	51.8	

Method	Modality	Accuracy (%)
VS-CNN [22]	Skeleton	29.0
JOULE [21] (by [22])	RGB	31.0
ResNeXt-101 [17] (by [22])	RGB	32.0
Real [consec]	RGB	36.1
Real	RGB	49.4
Synth+Real	RGB	67.8

Table 5. UESTC dataset Cross View I protocol, i.e. training on 1 viewpoint and testing on all the others. The rows and columns of the matrices correspond to training and testing views, respectively. We obtain significant improvements over the state of the art, due to our non-consecutive frame sampling and synthetic training.

Method	Modality	V1	V3	V5	V7	Avg
VS-CNN [22]	Skeleton	87	58	60	87	73.0
JOULE [21] (by [22])	RGB	74	48	47	80	62.3
ResNeXt-101 [17] (by [22])	RGB	52	44	48	52	49.0
Real [consec]	RGB	92.1	80.9	85.5	86.1	86.2
Real	RGB	91.3	86.8	89.4	88.9	89.1
Synth+Real	RGB	94.4	90.2	91.8	92.2	92.2

Table 6. UESTC dataset Cross View II protocol, i.e. training on 4 even viewpoints, testing on 4 odd viewpoints. Synthetic+Real training outperforms again the Real baseline.

Comparison with the state of the art. In the following, we employ the standard protocols for UESTC and NTU datasets, and compare our performance with other works. Tables 5 and 6 compare our results to the state-of-the-art methods reported by [22] on the recently released UESTC dataset, on CV-I and CV-II protocols. We outperform the RGB-based methods JOULE [21] and 3D ResNeXt-101 [17] by a large margin. We note that a first improvement can be attributed to our non-consecutive frame sampling strategy. Therefore, we report our consecutive real baseline as well. A significant performance boost is later obtained by having a mixture of synthetic and real training data. Using only RGB input, we obtain 18.4% improvement on the challenging CV-I protocol over real data (67.8 vs 49.4), and 35.8% improvement over the state of the art (67.8 vs 32.0). We also report on the odd test split of the CV-II protocol that has access to multi-view training data. The synthetic data again shows benefits over the real baselines. Compared to NTU, which contains object interactions that we do not simulate, the UESTC dataset focuses more on the anatomic movements, such as body exercises. We believe that these results convincingly demonstrate the generalization capability of our efficient synthetic data generation method to real body motion videos.

Method	Modality	CS	CV
Shahroudy 2016 [63] Part-LSTM	Skeleton	62.9	70.3
Liu 2016 [39] ST-LSTM	Skeleton	69.2	77.7
Liu 2016 [40] GCA-LSTM	Skeleton	74.4	82.8
Ke 2017 [27] MTLN	Skeleton	79.6	84.8
Liu 2017 [41] View-invariant	Skeleton	80.0	87.2
Baradel 2017 [3] Hands attention	RGB+Skeleton	84.8	90.6
Liu 2018 [42] Pose evolution	RGB+Depth	91.7	95.3
Baradel 2017 [3] Hands attention	RGB (Pose)	75.6	80.5
Liu 2018 [42] Pose evolution	RGB (Pose)	78.8	84.2
Zolfaghari 2017 [86] Multi-stream	RGB (Pose+Flow)	80.8	-
Luvizon 2018 [46] Multi-task	RGB (Pose)	85.5	-
Baradel 2018 [4] Glimpse clouds	RGB (Pose)	86.6	93.2
Wang 2018 [74] DA-Net	RGB (Flow)	88.1	92.0
Luo 2018 [45] Graph distillation	RGB (Pose+Flow+Depth)	89.5	-
Real RGB [consec]	RGB	86.3	90.8
Real RGB	RGB	89.0	93.1
Real Flow	RGB (Flow)	84.4	90.9
Real RGB+Flow	RGB (Flow)	90.0	94.3
Synth+Real RGB	RGB	89.6	94.1
Synth+Real Flow	RGB (Flow)	85.6	91.4
Synth+Real RGB+Flow	RGB (Flow)	90.7	95.0

Table 7. We report on the standard protocols of NTU for completeness. We improve previous RGB-based methods due to non-consecutive sampling and synthetic training. Additional cues extracted from RGB modality are denoted in parenthesis.

In Table 7, we compare our results to the state-of-the-art methods on standard NTU splits. Our results on both splits achieve state-of-the-art performance only with the RGB modality. In comparison, [4, 46, 86] use pose information during training. [45] uses other modalities from Kinect such as depth and skeleton during training. Similar to us, [74] uses a two-stream approach. Our non-consecutive sampling boosts the performance, and we have moderate gains with the synthetic data for both RGB and flow streams.

4.3. One-shot training

We test the limits of our approach on unconstrained videos of the Kinetics-15 dataset. These videos are challenging for several reasons. First, the 3D human motion estimation fails often due to complex conditions such as motion blur, low-resolution, occlusion, crowded scenes, and fast motion. Second, there exist cues about the action context that are difficult to simulate, such as object interactions, bias towards certain clothing or environments for certain actions. Assuming that body motions alone, even when noisy, provide discriminative information for actions, we augment the 15 training videos of one-shot Kinetics-15 subset synthetically (see Figure 6).

We use a pre-trained feature extractor model and only train a linear layer from the features to the 15 classes. We observe over-fitting with higher-capacity models due to limited one-shot training data. We experiment with two pre-trained models, obtained from [8]: RGB and flow. The models follow the 3D ResNeXt-101 architecture from [17] and are trained on Mini-Kinetics-200 categories with $16 \times 112 \times 112$ resolution with consecutive frame sampling. Table 8 shows that the performance of the real baseline is



Figure 6. Sample video frames from the one-shot Kinetics-15 dataset. We provide side-by-side illustrations for real frames and their synthetically augmented versions from the original viewpoint. Note that we render the synthetic body on a static background for computational efficiency, but augment it during training with random real videos by using the segmentation mask.

Training data	Synth background	Accuracy (%)		
		RGB	Flow	RGB+Flow
Real	-	26.2	20.6	28.4
Real + Synth	LSUN images	26.3	21.1	29.2
Real + Synth	Mini-Kinetics videos	32.7	22.3	34.6

Table 8. Performance on the one-shot Kinetics-15 dataset. Real training data consists of 1 training sample per category, i.e. 15 videos. We augment the training data with synthetically rendered SMPL sequences extracted from real data, blended on random backgrounds from the Mini-Kinetics training videos and obtain 6.5% improvement over training only with real data. We train only the last linear layer of the ResNeXt-101 3D CNN model pre-trained on Mini-Kinetics 200 classes.

very low (26.2% for RGB). We obtain $\sim 6\%$ improvement by adding synthetic data. We also experiment with static background images from the LSUN dataset [79] and note the importance of realistic noisy backgrounds for generalization to in-the-wild videos. The relatively small improvement can be explained by the fact that the pre-trained features might not capture the synthetic domain, preventing the classifier from exploiting effectively the additional data.

5. Conclusions

We presented an effective methodology for automatically augmenting action recognition datasets with synthetic videos. We explored the importance of different variations in the synthetic data, such as viewpoints and motions. Our analysis emphasizes the question on how to diversify motions within an action category. We obtain significant improvements for action recognition from unseen viewpoints and one-shot training. However, our approach is limited by the performance of the 3D pose estimation, which can fail in cluttered scenes. Possible future directions include action-conditioned generative models for motion sequences and simulation of contextual cues for action recognition.

Acknowledgements. This work was supported in part by Google AI, EPSRC grant ExToI, Louis Vuitton ENS Chair on Artificial Intelligence, and DGA project DRAAF.

References

- [1] Carnegie-Mellon Mocap Database. <http://mocap.cs.cmu.edu/>. 2, 4
- [2] Norman I. Badler, Cary B. Phillips, and Bonnie Lynn Webber. *Simulating Humans: Computer Graphics Animation and Control*. Oxford University Press, Inc., New York, NY, USA, 1993. 2
- [3] Fabien Baradel, Christian Wolf, and Julien Mille. Pose-conditioned spatio-temporal attention for human action recognition. *CoRR*, abs/1703.10106, 2017. 3, 8
- [4] Fabien Baradel, Christian Wolf, Julien Mille, and Graham W. Taylor. Glimpse clouds: Human activity recognition from unstructured feature points. In *CVPR*, 2018. 8
- [5] Federica Bogo, Angjoo Kanazawa, Christoph Lassner, Peter Gehler, Javier Romero, and Michael J. Black. Keep it SMPL: Automatic estimation of 3D human pose and shape from a single image. In *ECCV*, 2016. 3
- [6] João Carreira and Andrew Zisserman. Quo vadis, action recognition? A new model and the Kinetics dataset. In *CVPR*, 2017. 1, 4
- [7] Wenzheng Chen, Huan Wang, Yangyan Li, Hao Su, Zhenhua Wang, Changhe Tu, Dani Lischinski, Daniel Cohen-Or, and Baoquan Chen. Synthesizing training images for boosting human 3D pose estimation. In *3DV*, 2016. 2
- [8] Nieves Crasto, Philippe Weinzaepfel, Karteek Alahari, and Cordelia Schmid. MARS: Motion-augmented RGB stream for action recognition. In *CVPR*, 2019. 8
- [9] César Roberto De Souza, Adrien Gaidon, Yohann Cabon, and Antonio M. López Peña. Procedural generation of videos to train deep action recognition networks. In *CVPR*, 2017. 2, 7
- [10] Carl Doersch and Andrew Zisserman. Sim2real transfer learning for 3D pose estimation: motion to the rescue. *CoRR*, abs/1907.02499, 2019. 13, 14
- [11] Alexey Dosovitskiy, Philipp Fischer, Eddy Ilg, Philip Hausser, Caner Hazirbas, Vladimir Golkov, Patrick van der Smagt, Daniel Cremers, and Thomas Brox. FlowNet: Learning optical flow with convolutional networks. In *ICCV*, 2015. 1
- [12] Hao-Shu Fang, Shuqin Xie, Yu-Wing Tai, and Cewu Lu. RMPE: Regional multi-person pose estimation. In *ICCV*, 2017. 3, 4
- [13] Ali Farhadi and Mostafa K. Tabrizi. Learning to recognize activities from the wrong view point. In *ECCV*, 2008. 3
- [14] Christoph Feichtenhofer, Haoqi Fan, Jitendra Malik, and Kaiming He. SlowFast networks for video recognition. In *ICCV*, 2019. 1, 4
- [15] Christoph Feichtenhofer, Axel Pinz, and Andrew Zisserman. Convolutional two-stream network fusion for video action recognition. In *CVPR*, 2016. 1
- [16] Mona Fathollahi Ghezalghieh, Rangachar Kasturi, and Sudeep Sarkar. Learning camera viewpoint using CNN to improve 3D body pose estimation. In *3DV*, 2016. 2
- [17] Kensho Hara, Hirokatsu Kataoka, and Yutaka Satoh. Can spatiotemporal 3D CNNs retrace the history of 2D CNNs and ImageNet? In *CVPR*, 2018. 1, 4, 7, 8, 14, 15
- [18] Yana Hasson, Gül Varol, Dimitrios Tzionas, Igor Kalevatykh, Michael J. Black, Ivan Laptev, and Cordelia Schmid. Learning joint reconstruction of hands and manipulated objects. In *CVPR*, 2019. 2
- [19] Sepp Hochreiter and Jürgen Schmidhuber. Long short-term memory. *Neural Computation*, 9(8):1735–1780, 1997. 2
- [20] David T. Hoffmann, Dimitrios Tzionas, Michael J. Black, and Siyu Tang. Learning to train with synthetic humans. In *GCPR*, 2019. 2
- [21] Jian-Fang Hu, Wei-Shi Zheng, Jianhuang Lai, and Zhang Jianguo. Jointly learning heterogeneous features for RGB-D activity recognition. *IEEE Transactions on Pattern Analysis and Machine Intelligence*, 39(11):2186–2200, 2017. 7, 14, 15
- [22] Yanli Ji, Feixiang Xu, Yang Yang, Fumin Shen, Hen Tao Shen, and Weishi Zheng. A large-scale RGB-D database for arbitrary-view human action recognition. In *ACMMM*, 2018. 2, 5, 7, 14, 15
- [23] Imran N. Junejo, Emilie Dexter, Ivan Laptev, and Patrick Perez. View-independent action recognition from temporal self-similarities. *IEEE Transactions on Pattern Analysis and Machine Intelligence*, 33(1):172–185, 2011. 1
- [24] Angjoo Kanazawa, Michael J. Black, David W. Jacobs, and Jitendra Malik. End-to-end recovery of human shape and pose. In *CVPR*, 2018. 3
- [25] Angjoo Kanazawa, Jason Y. Zhang, Panna Felsen, and Jitendra Malik. Learning 3D human dynamics from video. In *CVPR*, 2019. 2, 3, 12
- [26] Will Kay, Joao Carreira, Karen Simonyan, Brian Zhang, Chloe Hillier, Sudheendra Vijayanarasimhan, Fabio Viola, Tim Green, Trevor Back, Paul Natsev, Mustafa Suleyman, and Andrew Zisserman. The Kinetics human action video dataset. *CoRR*, abs/1705.06950, 2017. 5
- [27] Qihong Ke, Mohammed Bennamoun, Senjian An, Ferdous Sohel, and Farid Boussaid. A new representation of skeleton sequences for 3D action recognition. In *CVPR*, 2017. 2, 8
- [28] Nikos Kolotouros, Georgios Pavlakos, and Kostas Daniilidis. Convolutional mesh regression for single-image human shape reconstruction. In *CVPR*, 2019. 3
- [29] Yu Kong, Zhengming Ding, Jun Li, and Yun Fu. Deeply learned view-invariant features for cross-view action recognition. *IEEE Transactions on Image Processing*, 26(6):3028–3037, 2017. 3
- [30] Yu Kong and Yun Fu. Human action recognition and prediction: A survey. *CoRR*, abs/1806.11230, 2018. 2
- [31] Christoph Lassner, Javier Romero, Martin Kiefel, Federica Bogo, Michael J. Black, and Peter V. Gehler. Unite the people: Closing the loop between 3D and 2D human representations. In *CVPR*, 2017. 3
- [32] Yann LeCun, Bernhard E. Boser, John S. Denker, Donnie Henderson, Richard E. Howard, Wayne E. Hubbard, and Lawrence D. Jackel. Backpropagation applied to handwritten zip code recognition. *Neural Computation*, 1(4):541–551, 1989. 1

- [33] Junnan Li, Yongkang Wong, Qi Zhao, and Mohan Kankanhalli. Unsupervised learning of view-invariant action representations. In *NeurIPS*, 2018. 2, 3
- [34] Wen Li, Zheng Xu, Dong Xu, Dengxin Dai, and Luc Van Gool. Domain generalization and adaptation using low rank exemplar SVMs. *IEEE Transactions on Pattern Analysis and Machine Intelligence*, 40(5):1114–1127, 2018. 2
- [35] Ji Lin, Chuang Gan, and Song Han. TSM: Temporal shift module for efficient video understanding. In *ICCV*, 2019. 1
- [36] Jian Liu, Naveed Akhtar, and Ajmal Mian. Temporally coherent full 3D mesh human pose recovery from monocular video. *CoRR*, abs/1906.00161, 2019. 2, 3, 7
- [37] Jian Liu, Hossein Rahmani, Naveed Akhtar, and Ajmal Mian. Learning human pose models from synthesized data for robust RGB-D action recognition. *International Journal of Computer Vision (IJCV)*, 2019. 2
- [38] Jingen Liu, Mubarak Shah, Benjamin Kuipers, and Silvio Savarese. Cross-view action recognition via view knowledge transfer. In *CVPR*, 2011. 1
- [39] Jun Liu, Amir Shahroudy, Dong Xu, and Gang Wang. Spatio-temporal LSTM with trust gates for 3D human action recognition. In *ECCV*, 2016. 2, 8
- [40] Jun Liu, Gang Wang, Ping Hu, Ling-Yu Duan, and Alex C. Kot. Global context-aware attention LSTM networks for 3D action recognition. In *CVPR*, 2017. 2, 8
- [41] Mengyuan Liu, Hong Liu, and Chen Chen. Enhanced skeleton visualization for view invariant human action recognition. *Pattern Recognition*, 68(C):346–362, 2017. 2, 8
- [42] Mengyuan Liu and Junsong Yuan. Recognizing human actions as the evolution of pose estimation maps. In *CVPR*, 2018. 3, 8
- [43] Yang Liu, Zhaoyang Lu, Jing Li, and Tao Yang. Hierarchically learned view-invariant representations for cross-view action recognition. *IEEE Transactions on Circuits and Systems for Video Technology*, 2019. 3
- [44] Matthew Loper, Naureen Mahmood, Javier Romero, Gerard Pons-Moll, and Michael J. Black. SMPL: A skinned multi-person linear model. In *SIGGRAPH Asia*, 2015. 2, 3
- [45] Zelun Luo, Jun-Ting Hsieh, Lu Jiang, Juan Carlos Niebles, and Li Fei-Fei. Graph distillation for action detection with privileged information. In *ECCV*, 2018. 8
- [46] Diogo C. Luvizon, David Picard, and Hedi Tabia. 2D/3D pose estimation and action recognition using multitask deep learning. In *CVPR*, 2018. 3, 8
- [47] Fengjun Lv and Ramakant Nevatia. Single view human action recognition using key pose matching and viterbi path searching. In *CVPR*, 2007. 2
- [48] Javier Marin, David Vazquez, David Geronimo, and Antonio M. Lopez. Learning appearance in virtual scenarios for pedestrian detection. In *CVPR*, 2010. 2
- [49] Iacopo Masi, Anh Tuan Tran, Tal Hassner, Gozde Sahin, and Gérard Medioni. Face-specific data augmentation for unconstrained face recognition. *International Journal of Computer Vision (IJCV)*, 2019. 2
- [50] Alejandro Newell, Kaiyu Yang, and Jia Deng. Stacked hourglass networks for human pose estimation. In *ECCV*, 2016. 4, 13
- [51] Mohamed Omran, Christoph Lassner, Gerard Pons-Moll, Peter V. Gehler, and Bernt Schiele. Neural body fitting: Unifying deep learning and model-based human pose and shape estimation. In *3DV*, 2018. 3
- [52] Georgios Pavlakos, Luyang Zhu, XiaoWei Zhou, and Kostas Daniilidis. Learning to estimate 3D human pose and shape from a single color image. In *CVPR*, 2018. 3
- [53] Leonid Pishchulin, Arjun Jain, Mykhaylo Andriluka, Thorsten Thormählen, and Bernt Schiele. Articulated people detection and pose estimation: Reshaping the future. In *CVPR*, 2012. 2
- [54] Will Price and Dima Damen. Retro-Actions: Learning ‘close’ by time-reversing ‘open’ videos. 2019. 16
- [55] Xavier Puig, Kevin Ra, Marko Boben, Jiaman Li, Tingwu Wang, Sanja Fidler, and Antonio Torralba. VirtualHome: Simulating household activities via programs. In *CVPR*, 2018. 2
- [56] Xuelin Qian, Yanwei Fu, Tao Xiang, Wenxuan Wang, Jie Qiu, Yang Wu, Yu-Gang Jiang, and Xiangyang Xue. Pose-normalized image generation for person re-identification. In *ECCV*, 2018. 2
- [57] Hossein Rahmani, Arif Mahmood, Du Huynh, and Ajmal Mian. Histogram of oriented principal components for cross-view action recognition. *IEEE Transactions on Pattern Analysis and Machine Intelligence*, 38(12):2430–2443, 2016. 2
- [58] Hossein Rahmani and Ajmal Mian. Learning a non-linear knowledge transfer model for cross-view action recognition. In *CVPR*, 2015. 2
- [59] Hossein Rahmani and Ajmal Mian. 3D action recognition from novel viewpoints. In *CVPR*, 2016. 2
- [60] Hossein Rahmani, Ajmal Mian, and Mubarak Shah. Learning a deep model for human action recognition from novel viewpoints. *IEEE Transactions on Pattern Analysis and Machine Intelligence*, 40(3):667–681, 2018. 2, 3
- [61] Javier Romero, Matthew Loper, and Michael J. Black. FlowCap: 2D human pose from optical flow. In *GCPR*, 2015. 13
- [62] Hiroaki Sakoe and Seibi Chiba. Dynamic programming algorithm optimization for spoken word recognition. *IEEE Transactions on Acoustics, Speech, and Signal Processing*, 26(1):43–49, 1978. 4
- [63] Amir Shahroudy, Jun Liu, Tian-Tsong Ng, and Gang Wang. NTU RGB+D: A large scale dataset for 3D human activity analysis. In *CVPR*, 2016. 1, 2, 5, 8
- [64] Jamie Shotton, Andrew Fitzgibbon, Mat Cook, Toby Sharp, Mark Finocchio, Richard Moore, Alex Kipman, and Andrew Blake. Real-time human pose recognition in parts from single depth images. In *CVPR*, 2011. 1, 2
- [65] Karen Simonyan and Andrew Zisserman. Two-stream convolutional networks for action recognition in videos. In *NeurIPS*, 2014. 4, 13
- [66] Khurram Soomro, Amir Roshan Zamir, and Mubarak Shah. UCF101: A dataset of 101 human actions classes from videos in the wild. *CRCV-TR-12-01*, 2012. 1
- [67] Hao Su, Charles R. Qi, Yangyan Li, and Leonidas J. Guibas. Render for CNN: Viewpoint estimation in images using CNNs trained with rendered 3D model views. In *ICCV*, 2015. 1

- [68] SURREACT project page. <http://www.di.ens.fr/willow/research/surreact/>. 2, 12, 18
- [69] Tijmen Tieleman and Geoffrey Hinton. Lecture 6.5—RMSprop: Divide the gradient by a running average of its recent magnitude. COURSERA: Neural Networks for Machine Learning, 2012. 5
- [70] Du Tran, Lubomir Bourdev, Rob Fergus, Lorenzo Torresani, and Manohar Paluri. Learning spatiotemporal features with 3D convolutional networks. In *ICCV*, 2015. 4
- [71] Hsiao-Yu Fish Tung, Hsiao-Wei Tung, Ersin Yumer, and Katerina Fragkiadaki. Self-supervised learning of motion capture. In *NeurIPS*, 2017. 3
- [72] Gül Varol, Duygu Ceylan, Bryan Russell, Jimei Yang, Ersin Yumer, Ivan Laptev, and Cordelia Schmid. BodyNet: Volumetric inference of 3D human body shapes. In *ECCV*, 2018. 2, 3
- [73] Gül Varol, Javier Romero, Xavier Martin, Naureen Mahmood, Michael J. Black, Ivan Laptev, and Cordelia Schmid. Learning from synthetic humans. In *CVPR*, 2017. 1, 2, 3, 4, 14, 15
- [74] Dongang Wang, Wanli Ouyang, Wen Li, and Dong Xu. Dividing and aggregating network for multi-view action recognition. In *ECCV*, 2018. 2, 3, 8
- [75] Jiang Wang, Xiaohan Nie, Yin Xia, Ying Wu, and Song-Chun Zhu. Cross-view action modeling, learning, and recognition. In *CVPR*, 2014. 2
- [76] Limin Wang, Yuanjun Xiong, Zhe Wang, Yu Qiao, Dahua Lin, Xiaoou Tang, and Luc Van Gool. Temporal segment networks: Towards good practices for deep action recognition. In *ECCV*, 2016. 1, 4
- [77] Daniel Weinland, Edmond Boyer, and Remi Ronfard. Action recognition from arbitrary views using 3D exemplars. In *ICCV*, 2007. 2
- [78] Saining Xie, Chen Sun, Jonathan Huang, Zhuowen Tu, and Kevin Murphy. Rethinking spatiotemporal feature learning: Speed-accuracy trade-offs in video classification. In *ECCV*, 2017. 5
- [79] Fisher Yu, Yinda Zhang, Shuran Song, Ari Seff, and Jianxiong Xiao. LSUN: Construction of a large-scale image dataset using deep learning with humans in the loop. *CoRR*, abs/1506.03365, 2015. 8, 15
- [80] Alan L. Yuille and Chenxi Liu. Deep nets: What have they ever done for vision? *CoRR*, abs/1805.04025, 2018. 2
- [81] Dingwen Zhang, Guangyu Guo, Dong Huang, and Junwei Han. PoseFlow: A deep motion representation for understanding human behaviors in videos. In *CVPR*, 2018. 3, 4
- [82] Pengfei Zhang, Cuiling Lan, Junliang Xing, Wenjun Zeng, Jianru Xue, and Nanning Zheng. View adaptive recurrent neural networks for high performance human action recognition from skeleton data. In *ICCV*, 2017. 2
- [83] Jingjing Zheng and Zhuolin Jiang. Learning view-invariant sparse representations for cross-view action recognition. In *ICCV*, 2013. 3
- [84] Jingjing Zheng, Zhuolin Jiang, and Rama Chellappa. Cross-view action recognition via transferable dictionary learning. *IEEE Transactions on Image Processing*, 25(6):2542–2556, 2016. 1, 3
- [85] Christian Zimmermann and Thomas Brox. Learning to estimate 3D hand pose from single RGB images. In *ICCV*, 2017. 1, 2
- [86] Mohammadreza Zolfaghari, Gabriel L. Oliveira, Nima Sedaghat, and Thomas Brox. Chained multi-stream networks exploiting pose, motion, and appearance for action classification and detection. In *ICCV*, 2017. 3, 8, 15

APPENDIX

This appendix provides detailed explanations for several components of our approach (Section A). We also report complementary results for the flow stream, synthetic training, and our non-consecutive frame sampling strategy (Section B). Finally, we illustrate our SURREACT dataset with more visual samples (Section C). A supplemental video at the project page [68] also provides video samples from our dataset.

A. Implementation details

Motion sequence interpolation. As explained in Section 3.2 of the main paper, we explore creating new sequences by interpolating pairs of motions from the same action category. Here, we visually illustrate this process. Figure A.1 shows two sequences of *sitting down* that are first aligned with dynamic time warping, and then linearly interpolated. We only experiment with equal weights when interpolating (i.e. 0.5), but one can sample different weights when increasing the number of sequences further.

3D translation in SURREACT. In Section 3.2 of the main paper, we explained that we translate the people in the xy image plane only when there are multiple people in the scene. HMMR [25] estimates the weak-perspective camera scale, jointly with the body pose and shape. We note that obtaining 3D translation of the person in the camera coordinates is an ambiguous problem. It requires the size of the person to be known.

HMMR relies on 2D pose estimation to locate the bounding box of the person which then becomes the input to a CNN. The CNN outputs a scale estimation s_b together with the $[x_b, y_b]$ normalized image coordinates of the person center with respect to the bounding box. We first convert these values to be with respect to the original uncropped image: s and $[x, y]$. We can recover an approximate value for the z coordinate of the person center, by assuming a fixed focal length $F = 500$. The translation in z then becomes: $z = F / (0.5 * W * s)$, where W is the image resolution and s is the estimated camera scale. The translation of the person center then becomes $[x, y, z]$. In practice, the z values are very noisy whereas $[x, y]$ values are more reliable. We therefore assume that the person is always centered at $z = 0$ and apply the translation only in the xy plane.

We observe that due to the noisy 2D person detections the estimated translation is noisy even in the xy image plane, leading to less generalization performance on real

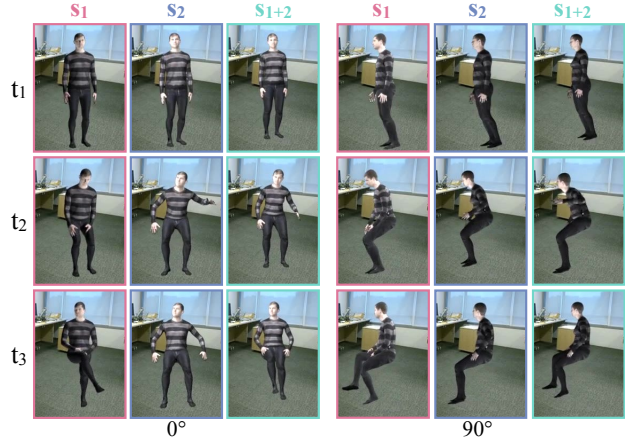


Figure A.1. Motion interpolation procedure for the *sitting* action. Two temporally aligned sequences s_1 and s_2 from different individuals are interpolated to create s_{1+2} , from two viewpoints. Note the new arm and leg angles that contribute to motion diversity.

#people	translation	0°	45°	90°
single	xyz	18.3	17.8	15.0
multi	xyz	21.0	21.2	17.3
multi	xy	26.8	26.0	21.9
multi	xy (when multi-person)	28.5	27.2	23.0

Table A.1. Training on different versions of the synthetic data generated from 10 sequences per action from the NTU CVS protocol. We train only on synthetic and test on the real test set. Multi-person videos in the synthetic training improves performance, especially in the interaction categories (see Figure A.7). The noisy translation estimates degrades generalization, therefore, we use only xy translation and only in the case of multi-person. See text for further details.

data when we train only with synthetic data. We validate this empirically in Table A.1. We render multiple versions of the synthetic dataset with 10 motion sequences per action, each rendered from 8 viewpoints. We train only with this synthetic data and evaluate on the real NTU CVS protocol. Including multiple people improves performance (first and second rows), mainly because 11 out of 60 action categories in NTU are two-person interactions. Figure A.7 also shows the confusion matrix of training only with single-person, resulting in the confusion of the interaction categories. Dropping the z component from the translation further improves (second and third rows). We also experiment with no translation if there is a single person, and xy translation only for the multi-person case (fourth row), which

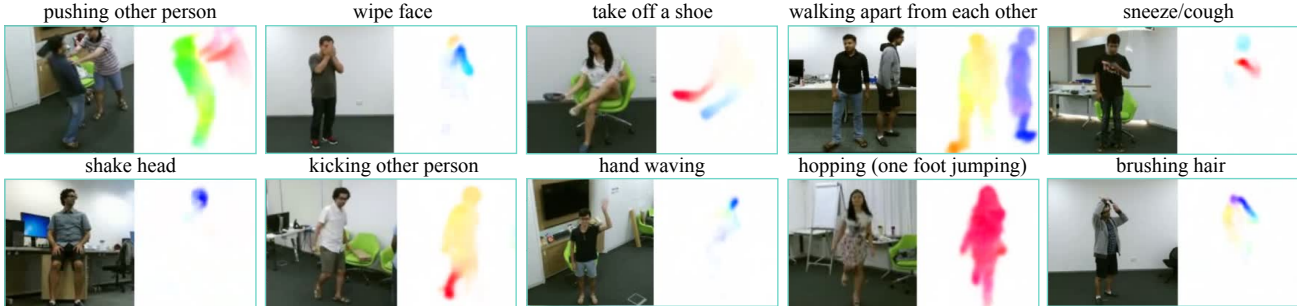


Figure A.2. Qualitative results for our optical flow estimation network trained on SURREACT, tested on the NTU dataset.

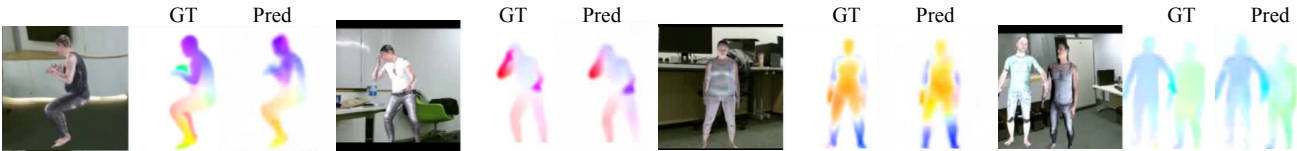


Figure A.3. Qualitative results for our optical flow estimation network trained and tested on SURREACT, together with the ground truth.

has the best generalization performance. This is unintuitive since some actions such as *jumping* are not realistic when the vertical translation is not simulated. This indicates that the translation estimations from the real data need further improvement to be incorporated in the synthetic data. Our 3D CNN is otherwise sensitive to the temporal jitter induced by the noisy translations of the people.

Flow estimation. We train our own optical flow estimation CNN, which we use to compute the flow in an on-line fashion, during action classification training. In other words, we do not require pre-processing the videos for training. To do so, we use a light-weight stacked hourglass architecture [50] with two stacks. The input and output have 256×256 and 64×64 spatial resolution, respectively. The input consists of 2 consecutive RGB frames of a video, the output is the downsampled optical flow ground truth. We train with mean squared error between the estimated and ground truth flow values. We obtain the ground truth from our synthetic SURREACT dataset. Qualitative results of our optical flow estimates can be seen in Figures A.2 and A.3 on real and synthetic images, respectively. When we compute the flow *on-the-fly* for action recognition, we loop over the 16-frame RGB input to compute the flow between every 2 frames and obtain 15-frame flow field as input to the action classification network.

Training details. We give additional details to Section 3.3 of the main paper on the action classification training. We train our networks for 50 epochs with an initial learning rate of 10^{-3} which is decreased twice with a factor of 10^{-1} at epochs 40 and 45, respectively. For NTU, UESTC, and SURREACT datasets, we spatially crop video frames

around the person bounding box with random augmentations in scale and the center of the bounding box. For the Kinetics dataset, we crop randomly with a bias towards the center. We scale the RGB values between $[0, 1]$ and jitter the color channels with a multiplicative coefficient randomly generated between $[0.8, 1.2]$ for each channel. We subtract 0.5 and clip the values between $[-0.5, 0.5]$ before inputting to the CNN.

B. Additional analyses

We present the results of the flow stream on the NTU CSV protocol, and the UESTC dataset (Section B.1). We analyze further the synthetic training (Section B.2). We define a synthetic test set and report the results of the models in the main paper also on this test set. We present additional ablations. We report the confusion matrix on the synthetic test set, as well as on the real test set, which allows us to gain insights about which action categories can be represented better synthetically. Finally, we explore the proposed non-consecutive sampling more in Section B.3.

B.1. Flow stream

Optical flow is widely used as input to action recognition networks [65]. It is also found to reduce the domain gap between synthetic and real data for 2D [61] and 3D [10] human pose estimation tasks. However, in our case, we do not observe significant gains by the flow stream.

Due to space constraints, we did not include the results of the optical flow stream for all datasets. Here, we report the results for the NTU CSV protocol, and the UESTC dataset.

NTU CSV protocol. Table A.2 presents results of the RGB+Flow fusion on the NTU CSV protocol for synth-

Training data		seen view		
		0°	45°	90°
RGB	Synth(0°:45°:360°)	54.0	49.5	42.7
	Real(0°)	86.9	74.5	53.6
	Synth(0°:45°:360°) + Real(0°)	89.1	82.0	67.1
Flow	Synth(0°:45°:360°)	51.7	46.9	38.6
	Real(0°)	82.8	70.6	49.7
	Synth(0°:45°:360°) + Real(0°)	85.9	76.4	58.9
RGB + Flow	Synth(0°:45°:360°)	60.6	55.5	47.8
	+ Real(0°)	88.8	78.2	57.3
Flow	Synth(0°:45°:360°) + Real(0°)	90.5	83.3	68.0

Table A.2. We report the RGB+Flow results on the NTU CVS protocol, complementary to the RGB-only results in Table 2 of the main paper. We have marginal improvements with flow unlike in other tasks where flow has been used to reduce the synthetic-real domain gap [10]. On the other hand, Synth+Real training consistently improves over the Real baseline also for the flow stream.

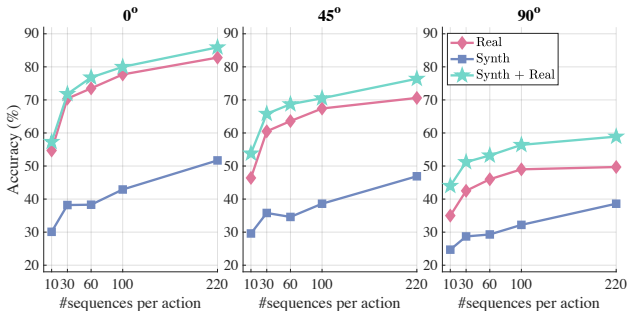


Figure A.4. The number of real sequences per action for: Real, Synth, Synth+Real training on NTU CVS split with the flow stream. The conclusions are the same as in Figure 5 of the main paper. Additional synthetic data (green) improves the accuracy especially for unseen viewpoints.

only, real-only, and the combination as in Table 2 of the main paper. Note that synthetic-only training reaches 60% performance on the 0° seen view without any real video.

Figure A.4 plots the number of sequences versus accuracy for the flow stream (similar to Figure 5 of the main paper). The performance of the flow stream is generally lower than the RGB stream, possibly due to the fine-grained categories which cannot be distinguished with coarse motion fields. But the Synth+Real setting consistently outperforms the Real baseline also for the flow input.

UESTC dataset. Table A.3 and A.4 report the RGB+Flow fusion on CV-I and CV-II protocols, respectively. In Table A.4, we also report the even test split on UESTC. We reported the odd test split in Table 6 of the main paper due to space constraints. The results indicate that the additional synthetic data helps also for the flow stream on UESTC. The late fusion of RGB+Flow obtains the best results.

We also note that we have trained a ResNeXt-101 architecture [17] with our implementation and obtained better

Method	Modality	Accuracy (%)	
VS-CNN [22]	Skeleton	29.0	
JOULE [21] (by [22])	RGB	31.0	
ResNeXt-101 [17] (by [22])	RGB	32.0	
ResNeXt-101 [17] (ours)	RGB	45.2	
RGB	Real [consec]	RGB	36.1
RGB	Real	RGB	49.4
	Synth + Real	RGB	67.8
Flow	Real	RGB	63.5
	Synth + Real	RGB	70.2
RGB + Flow	Real	RGB	63.2
	Synth + Real	RGB	74.5

Table A.3. UESTC dataset Cross View I protocol, i.e. training on one viewpoint and testing on all the others.

results than our ResNet-50 architecture (45.2% vs 36.1% on CV-I, 82.5% vs 76.1% on CV-II). This contradicts the results reported in [22].

B.2. Synthetic-only training

Here, we define a synthetic test set based on the NTU actions, and perform additional ablations on our synthetic data such as different input modalities beyond RGB and flow, effect of backgrounds, effect of further camera augmentations, and confusion matrix analysis.

Synthetic test set. Similar to SURREAL [73], we separate the assets such as cloth textures, body shapes, backgrounds into train and test splits, which allows us to validate our experiments also on a synthetic test set. Here, we use one sequence per action from the real 0° test set to generate a small synthetic test set, i.e. 60 motion sequences in total, rendered for the 8 viewpoints, using the test set assets.

We report the performance of our models from Tables 3 and 4 of the main paper on this set. Table A.5 confirms that the viewpoints should match between training and test for best results. Augmenting with all 8 views benefits the overall results. Table A.6 presents the gains obtained by motion augmentations on the synthetic test set. Both interpolations and the additive noise improves over applying no augmentation.

Different input types. The advantage of having a synthetic dataset is to be able to perform experiments with different modalities. Specifically, we have ground-truth optical flow, body-part segmentation for each video. We compare training with these input modalities as opposed to RGB, or the estimated flow in Table A.7. We evaluate on the real NTU CSV test set when applicable, and on the synthetic test set. We see that even when ground truth, the

Training views:			V1, V3, V5, V7					FV, V2, V4, V6					
Test views:			FV	V2	V4	V6	Avg _{even}	V1	V3	V5	V7	Avg _{odd}	Avg
VS-CNN [22]	Skeleton	RGB	87.0	54.0	71.0	60.0	68.0	87.0	58.0	60.0	87.0	73.0	70.5
Joule [21] (by [22])	RGB	RGB	74.0	49.0	57.0	55.0	58.8	74.0	48.0	47.0	80.0	62.3	60.6
ResNeXt [17] (by [22])	RGB	RGB	51.0	40.0	54.0	39.0	46.0	52.0	44.0	48.0	52.0	49.0	47.5
ResNeXt [17] (ours)	RGB	RGB	78.0	71.7	79.4	65.4	73.6	94.0	91.3	89.9	89.9	91.3	82.5
RGB	Real [consec]	RGB	78.1	63.1	76.6	46.4	66.1	92.1	80.9	85.5	86.1	86.2	76.1
RGB	Real	RGB	69.9	57.1	79.1	51.1	64.3	91.3	86.8	89.4	88.9	89.1	76.7
	Synth + Real	RGB	77.5	72.0	80.8	67.0	74.3	94.4	90.2	91.8	92.2	92.2	83.3
Flow	Real	RGB	73.5	68.4	81.2	60.3	70.9	94.6	83.4	89.8	90.8	89.7	80.3
	Synth + Real	RGB	74.7	67.0	82.3	63.6	71.9	94.8	84.9	89.4	91.1	90.1	81.0
RGB + Flow	Real	RGB	74.5	68.4	82.4	59.4	71.2	95.8	88.9	91.4	92.3	92.1	81.7
	Synth + Real	RGB	79.7	75.1	84.8	70.6	77.6	96.1	90.9	92.3	94.8	93.5	85.6

Table A.4. UESTC dataset Cross View II protocol, i.e. training on 4 odd viewpoints, testing on 4 even viewpoints (left), and vice versa (right). We present the complete results on both splits and their average for the Flow stream, as well as the RGB+Flow late fusion. Real+Synth training consistently outperforms the Real baseline.

	Synth Test Views								Avg
	0°	45°	90°	135°	180°	225°	275°	315°	
0	81.7	41.7	10.0	43.3	40.0	30.0	10.0	50.0	38.3
45-315	58.3	65.0	36.7	53.3	43.3	48.3	50.0	66.7	52.7
90-270	15.0	35.0	61.7	23.3	13.3	35.0	56.7	33.3	34.2
All 8	78.3	73.3	61.7	68.3	73.3	75.0	65.0	71.7	70.8

Table A.5. The performance of the view-augmented models from Table 3 of the main paper on the synthetic test set. We train only with synthetic videos obtained from 60 sequences per action. We confirm that the viewpoints should match also for the synthetic test set. We report the viewpoint breakdown, as well as the average.

#sequences per action	#renders	motion augmentation	Synth All
10	1	-	55.4
10	6	-	55.0
10	6	interpolation	58.8
10	6	additive noise	57.7
60	1	-	70.8

Table A.6. The performance of the motion-augmented models from Table 4 of the main paper on the synthetic test set. We train only with synthetic videos obtained from 60 sequences per action. Both augmentation approaches improve over the baseline.

optical flow performs worse than RGB, indicating difficulty of distinguishing fine-grained actions only with flow fields. Body-part segmentation on the other hand, outperforms other modalities due to providing precise locations for each body part and an abstraction which reduces the gap between the training and test splits. In other words, body-part segmentation is independent of clothing, lighting, background effects, but only contains motion and body shape information. This result highlights that we can improve action recognition by improving body part segmentation as in [86].

Effect of backgrounds. As explained in Section 3.2 of the main paper, we use 2D background images from the

Input type	Real			Synth All
	0°	45°	90°	
Flow (Pred)	38.3	34.6	29.3	58.4
Flow (GT)	-	-	-	61.2
RGB	48.3	44.3	38.8	70.8
Body-part segm (GT)	-	-	-	71.7

Table A.7. Different input types when training only with synthetic data and testing on the synthetic test set, as well as the real NTU CVS test set when applicable. The data is generated from 60 sequences per action. The results indicate that body part segmentation can be an informative representation for action classification. Optical flow, even when ground truth (GT) is used, is less informative for fine-grained action classes in NTU.

Backgrounds	Real			Synth All
	0°	45°	90°	
random LSUN	39.1	37.3	32.5	70.8
random NTU	42.7	39.8	34.3	67.9
fixed NTU	48.3	44.3	38.8	70.8

Table A.8. Effect of synthetic data backgrounds for synthetic-only training. Results are reported both on the real NTU CVS set and the synthetic test set. The synthetic training is generated from 60 sequences per action. Matching the target background statistics improves generalization to real. See text for details.

target action recognition domain in our synthetic dataset. We perform an experiment whether this helps on the NTU CVS setup. The NTU dataset is recorded in a lab environment, therefore has specific background statistics. We train models by replacing the background pixels of our synthetic videos randomly by LSUN [73, 79] images or the original NTU images outside the person bounding boxes. Table A.8 summarizes the results. Using random NTU backgrounds outperform using random LSUN backgrounds. However, we note that the process of using the segmentation mask creates some unrealistic artifacts around the person, which might contribute to the performance degradation. We therefore use the fixed backgrounds from the original renderings in the rest of the experiments.

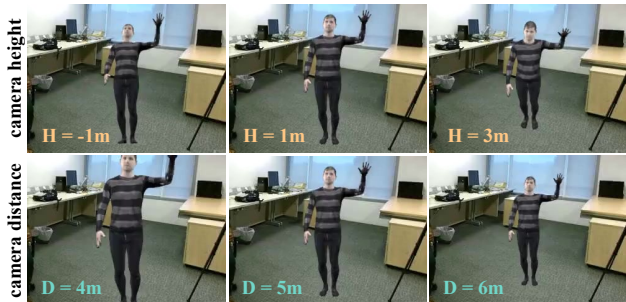


Figure A.5. We illustrate the limits for the camera height and distance parameters in SURREACT. We randomly sample between $[-1, 3]$ and $[4, 6]$ meters for the height and distance, respectively.

camera height & distance	0°	45°	90°
fixed	28.5	27.2	23.0
random	31.3	28.1	24.3

Table A.9. Training on different versions of the synthetic data generated from 10 sequences per action from the NTU CVS protocol. We ablate the importance of augmentations of the camera height and distance. We train only on synthetic and test on the real test set. We observe improvements with randomized camera positions besides the azimuth rotation.

Effect of camera height/distance augmentations. As stated in Section 3.2 of the main paper, we randomize the height and the distance of the camera to increase the view-point diversity within a certain azimuth rotation. We evaluate the importance of this with a controlled experiment in Table A.9. We render two versions of the synthetic training set with 10 sequences per action from 8 viewpoints. The first one has a fixed distance and height at 5 meters and 1 meter, respectively. In the second one, we randomly sample from $[4, 6]$ meters for the distance, and $[-1, 3]$ meters for the height. We see that the generalization to real NTU CVS dataset is improved with increased randomness in the synthetic training. Visuals corresponding to the pre-defined range can be found in Figure A.5.

Confusion matrices. We analyze two confusion matrices in Figure A.6: training only on the synthetic data and (i) testing on the synthetic test set; and (ii) testing on the real NTU CVS 0° view test set. The confused classes are highlighted on the figure. The confusions on both test sets suggest that the fine-grained action classes require more precise body motions, such as $\{clapping, rub\ two\ hands\ together\}$, and $\{reading, writing\}$. Other confusions include object interaction categories (e.g. $\{put\ on\ a\ hat, brushing\ hair\}$ and $\{typing\ on\ a\ keyboard, writing\}$), which can be explained by the fact that synthetic data does not simulate objects. These confusions are mostly resolved when training with both real and synthetic data.

	0°	45°	90°
Flow [consec]	80.6	68.3	44.7
Flow [non-consec]	82.8	70.6	49.7

Table A.10. Training and testing on the real NTU CVS split. We confirm that the non-consecutive sampling is beneficial also for the flow stream even though the flow estimates can be noisy between non-consecutive frames.

	Test mode					
	consec			non-consec		
	0°	45°	90°	0°	45°	90°
Train consec	83.9	67.9	42.9	27.5	20.6	13.8
Train non-consec	32.1	21.1	12.4	86.9	74.5	53.6

Table A.11. Training and testing on the real NTU CVS split. The frame sampling mode should be the same at training and test times.

	Test mode					
	ordered			non-ordered		
	0°	45°	90°	0°	45°	90°
Train ordered	86.9	74.5	53.6	16.4	13.1	8.1
Train non-ordered	67.2	50.2	32.8	72.7	57.8	37.2

Table A.12. Training and testing on the real NTU CVS split. Preserving the order of frames in non-consecutive sampling is important. The confusion matrix in Figure A.8 shows that the mistakes are often among ‘symmetric’ action classes such as *sitting up* and *standing up*. Order-aware models fail drastically when tested non-ordered, as expected.

B.3. Non-consecutive sampling

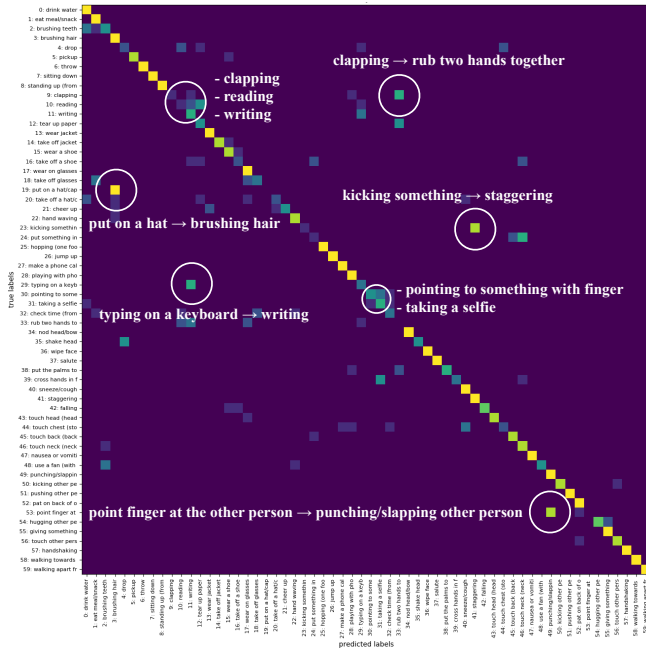
In this section, we explore the proposed frame sampling strategy further.

First, we confirm that the benefits of non-consecutive sampling applies also to the flow stream. Since flow is estimated online during training, we can compute flow between any two frames. Note that the flow estimation method is learned on 2 consecutive frames, therefore it produces noisy estimates for large displacements. However, even with this noise, in Table A.10, we demonstrate advantages of non-consecutive sampling over consecutive for the flow stream.

Next, we present our experiments about the testing modes as mentioned in Section 3.3 of the main paper. Table A.11 suggests that the training and testing modes should be the same for both consecutive and non-consecutive samplings. The convolutional filters adapt to certain training statistics, which should be preserved at test time.

Finally, we investigate the importance of the order of the frames when we randomly sample non-consecutively. We preserve the temporal order in all our experiments, except in Table A.12, where we experiment with a shuffled order. In this case, we observe a significant performance drop which can be explained by the confusion matrix in Figure A.8. The action classes such as *wearing* and *taking off* are heavily confused when the order is not preserved. This experiment allows detecting action categories that are temporally symmetric [54]. We also observe that the ordered model fails when tested in non-ordered mode, which indicates that the convolutional kernels become highly order-aware.

Train: Synth, Test: Synth



Train: Synth, Test: Real (0°)

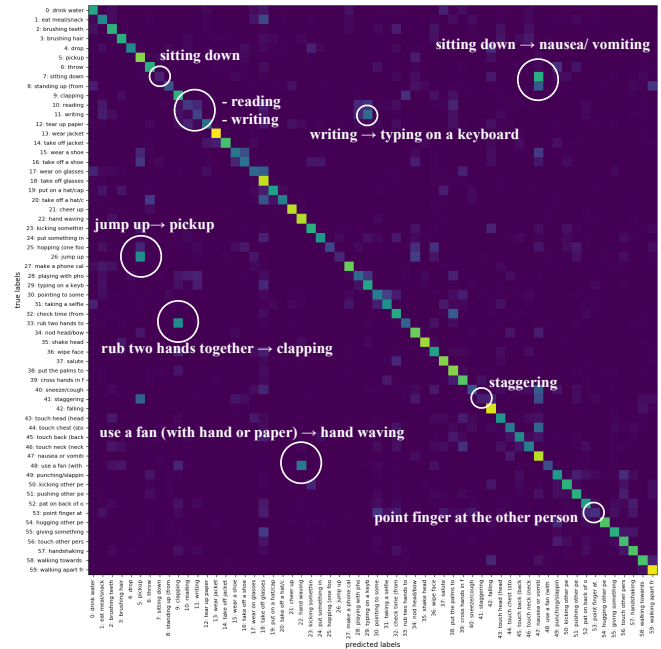


Figure A.6. The confusion matrices for training only with the final synthetic data with all the 220 sequences per action. Both on the synthetic test set (left) and the real 0° view test (right), the confusions are often between classes that are characterized by fine-grained body movements and object-interaction classes.

Train: Synth (single-person), Test: Real (0°)

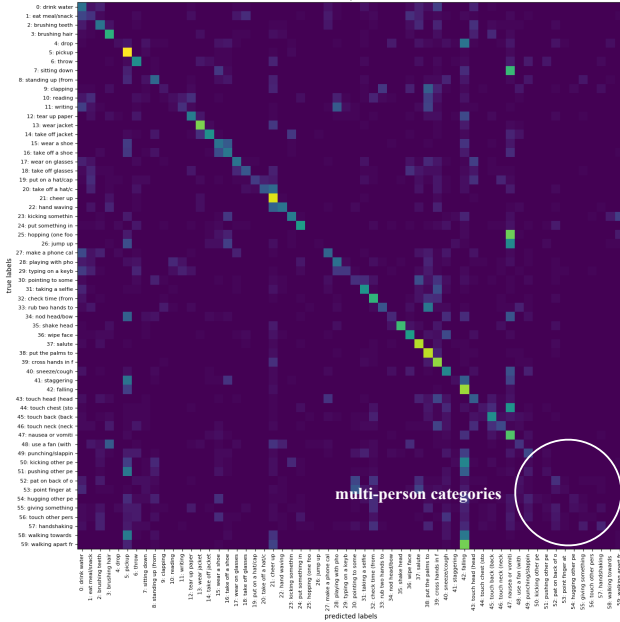


Figure A.7. We render a version of the synthetic data with 10 sequences per action, where we only insert a single person per video. When trained with this data, the two-person interaction categories (last 11 classes) are mostly misclassified on the real NTU CVS 0° view test data. The confusions suggest that it is important to model multi-person cases in the synthetic data.

Train/Test: Real 0° non-consec, non-ordered

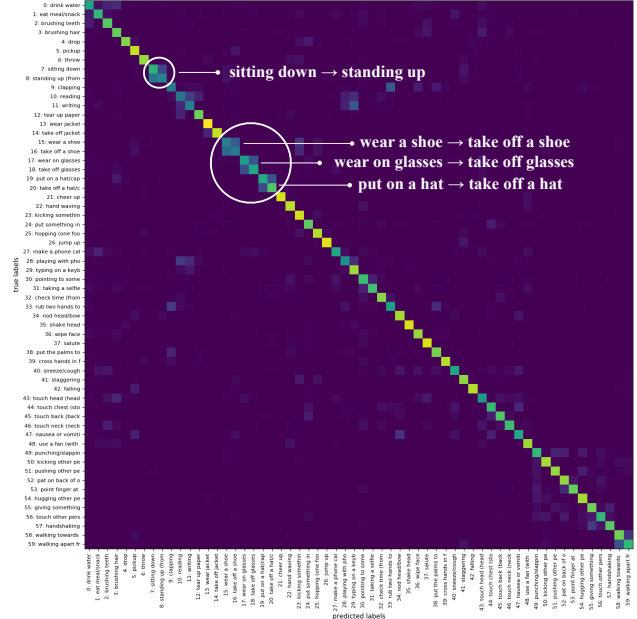


Figure A.8. We present the confusion matrix for the non-ordered training explained in Table A.12. The classes that require the temporal order to be distinguished are confused as expected. The training and test is performed on the real NTU CVS 0° view split.

C. SURREACT dataset illustrations

We provide visualizations for our SURREACT dataset in Figure A.9. The complete list of actions can be found in the supplemental video at [68].

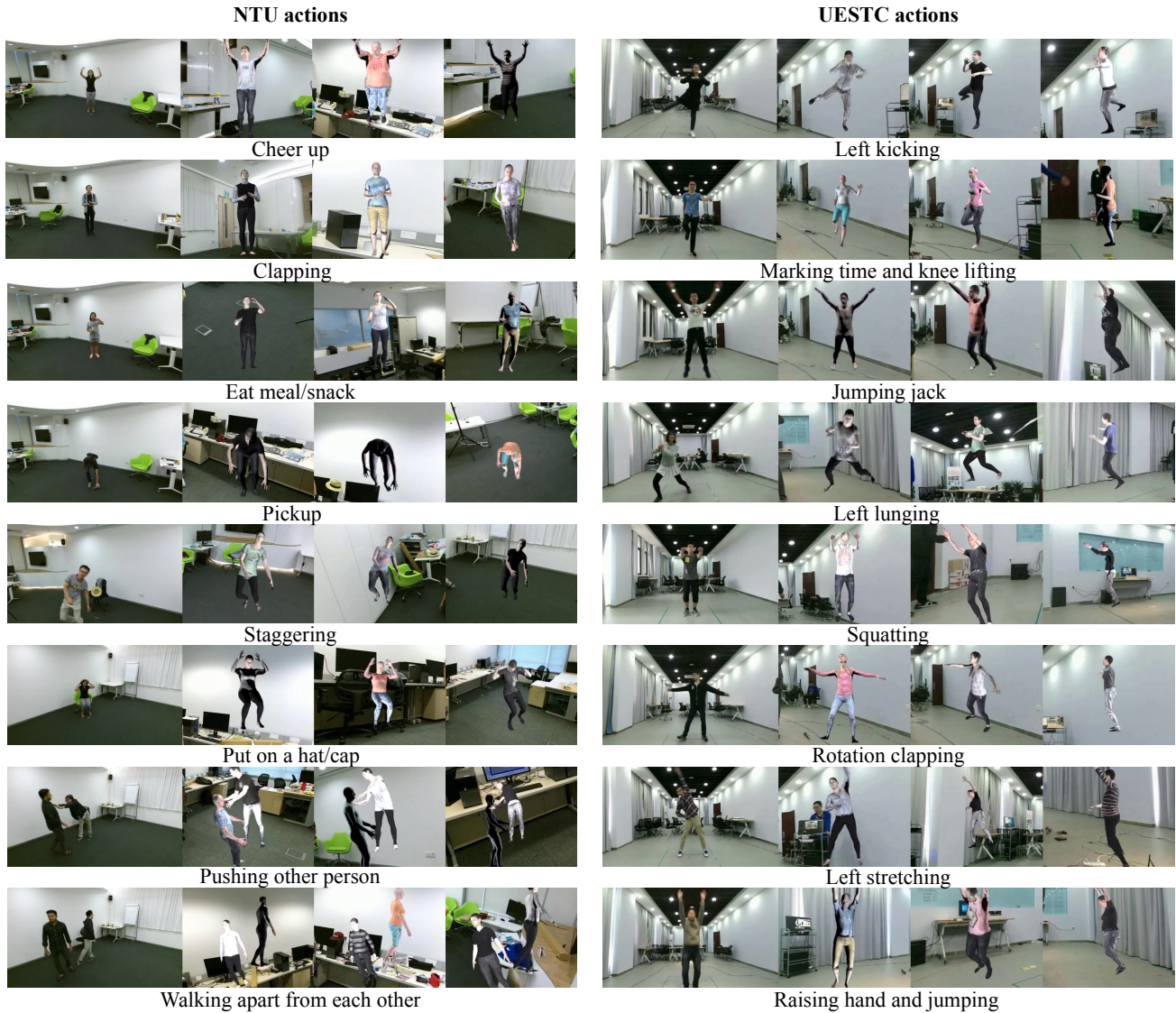


Figure A.9. We visualize samples from the SURREACT dataset for the actions from the NTU (left) and the UESTC (right) datasets. Each real video frame is accompanied with three synthetic augmentations. On the left, we show the variations in clothes, body shapes, backgrounds, camera height/distance from the original 0° viewpoint. On the right, we show the variations in viewpoints for 0°, 45°, and 90° views. More examples can be seen in the supplemental video at [68].